(12)

NOSC TR 1108

NOSC

NAVAL OCEAN SYSTEMS CENTER San Diego, California 92152-5000

Technical Report 1108
May 1986

Stationary/Slowly Moving Target Detection in Strong Background Clutter

Larry B. Stotts

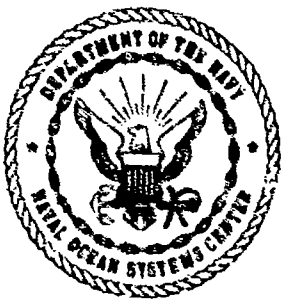

NAVAL OCEAN SYSTEMS CENTER

San Diego, California 92152-5000

F. M. PESTORIUS, CAPT, USN
Commander

R.M. HILLYER
Technical Director

ADMINISTRATIVE INFORMATION

The work described here was performed by the Electromagnetic Systems and Technology Division, Code 7402, Naval Ocean Systems Center, for the Space and Naval Warfare Systems Command.

Released by
L.B. Stotts, Associate
for Image Processing

Under authority of
R.L. Petty, Head
Electromagnetic Systems and
Technology Division

ACKNOWLEDGEMENTS

The author would like to thank Richard S. Cigledy and Scott Grier for their help in developing the image processing software used in this study, as well as assisting in the image analysis discussed. In addition, the author would like to acknowledge Richard Thompson, Space and Naval Warfare Command (SPAWAR 615), and Howard Stears, Defense Advanced Research Projects Agency, for their financial support and encouragement during the performance of the work described here.

JG

UNCLASSIFIED
SECURITY CLASSIFICATION OF THIS PAGE

AD-A172 225

REPORT DOCUMENTATION PAGE

1a. REPORT SECURITY CLASSIFICATION UNCLASSIFIED	1b. RESTRICTIVE MARKINGS
2a. SECURITY CLASSIFICATION AUTHORITY	3. DISTRIBUTION/AVAILABILITY OF REPORT
2b. DECLASSIFICATION/DOWNGRADING SCHEDULE	Approved for public release; distribution is unlimited.
4. PERFORMING ORGANIZATION REPORT NUMBER(S): NOSC TR 1108	5. MONITORING ORGANIZATION REPORT NUMBER(S)
6a. NAME OF PERFORMING ORGANIZATION Naval Ocean Systems Center	6b. OFFICE SYMBOL (If applicable) Code 7402
6c. ADDRESS (City, State and ZIP Code) San Diego, CA 92152-5000	7a. NAME OF MONITORING ORGANIZATION 7b. ADDRESS (City, State and ZIP Code)
8a. NAME OF FUNDING/SPONSORING ORGANIZATION Space and Naval Warfare Systems Command	8b. OFFICE SYMBOL (If applicable) SPAWAR-615
8c. ADDRESS (City, State and ZIP Code) Washington, DC 20363	9. PROCUREMENT INSTRUMENT IDENTIFICATION NUMBER 10. SOURCE OF FUNDING NUMBERS

PROGRAM ELEMENT NO.	PROJECT NO.	TASK NO.	Agency Accession No.
62712N	F12142	SX-34	DN388 563

11. TITLE (Include Security Classification)
Stationary/Slowly Moving Target Detection in Strong Background Clutter

12. PERSONAL AUTHOR(S)
Larry B. Stotts

13a. TYPE OF REPORT	13b. TIME COVERED	14. DATE OF REPORT (Year, Month, Day)	15. PAGE COUNT
Interim	FROM Oct 1984 TO Dec 1984	May 1986	44

16. SUPPLEMENTARY NOTATION

17. COSATI CODES			18. SUBJECT TERMS (Continue on reverse if necessary and identify by block number)
FIELD	GROUP	SUB-GROUP	Multispectral imagery Array sensor Maximum likelihood signal processing

19. ABSTRACT (Continue on reverse if necessary and identify by block number)

This report presents the maximum likelihood approach to nonmoving resolved/partially resolved target extraction from correlated images that can be extended to the underresolved, weak target case by restructuring the basic problem development in terms of the inherent two-dimensional aspects found in most remotely sensed images. The report also outlines the research required to extend application of the restructured development to an optimum processing approach for detecting stationary or slowly moving targets in clutter.

20. DISTRIBUTION/AVAILABILITY OF ABSTRACT	21. ABSTRACT SECURITY CLASSIFICATION
☒ UNCLASSIFIED/UNLIMITED ☐ SAME AS RPT ☐ DTIC USERS	UNCLASSIFIED

22a. NAME OF RESPONSIBLE INDIVIDUAL	22b. TELEPHONE (Include Area Code)	22c. OFFICE SYMBOL
Larry B. Stotts	(619) 225-7639	Code 7402

DD FORM 1473, 84 JAN

83 APR EDITION MAY BE USED UNTIL EXHAUSTED
ALL OTHER EDITIONS ARE OBSOLETE

UNCLASSIFIED
SECURITY CLASSIFICATION OF THIS PAGE

DD FORM 1473, 84 JAN

SUMMARY

The increasing sophistication of optical component and detector technology, combined with rapidly expanding surveillance requirements, suggests that infrared-based sensor systems may soon provide additional capability to the Navy in Fleet defense and intelligence gathering applications. The Defense Advanced Research Projects Agency (DARPA) has been pursuing the extension of Department of Defense surveillance capabilities during the past few years through the HI-resolution Calibrated Airborne Measurements (HI-CAMP) and TEAL RUBY programs, and these technologies are presently available to help assess the role of infrared (IR) sensors in the aforementioned roles. With the joint support of DARPA and the Naval Electronics System Command (Code 615), the Naval Ocean System Center (NOSC), her sister Centers, and the Naval Research Laboratory are currently developing a Navy Infrared Surveillance Data Base for assessing the utility of IR technology in Fleet defense, as well as other important Navy applications. This is a multifaceted program involving background clutter and target signature measurements, IR phenomenology modeling, and digital image processing.

An element of the Navy program involves the use of the TEAL RUBY Experiment to extract data relevant to Navy IR surveillance needs. These needs include weak and stationary targets. Notably, the TEAL RUBY sensor in its staring mode is severely limited for stationary target detection. The sensor suffers from high levels of pattern noise (on the order of 2 percent) even after calibration. Thus, techniques must be developed in the near future tc reduced image clutter and system noise, if Navy objectives for the TEAL RUBY Experiment are to be fulfilled. Accordingly, a task was initiated this fiscal year at NOSC to develop "optimum" image processing strategies for

A-1

detecting stationary and slowly moving, weak targets under various background conditions. This report outlines the interim results on this effort. Specifically, a mathematical approach for performing maximum likelihood detection of slowly moving/stationary targets from multispectral imagery is described, and its underlying assumptions are presented and discussed. Example DAEDALUS imagery is used to evaluate one of these assumptions in detail, and these results are presented.

CONTENTS

ILLUSTRATIONS

Figure

TABLES

1. INTRODUCTION

The increasing sophistication of optical component and detector technologies, combined with rapidly expanding remote sensing requirements, has sparked a commensurate development in exotic signal processing techniques for extracting desired information out of highly complex visible and infrared imagery[1]. At present, the most pressing problem in remote sensing for surveillance is underresolved, weak target detection in highly spatially structured optical imagery. The accepted approach to the extraction of targets in this case is to temporally band-pass the data through either an analog or digital filter, e.g., frame-to-frame subtraction. This technique is known to produce excellent results in the target signature. However, if the object of interest is stationary, or slowly moving, other means must be employed to identify and localize the target.

Several researchers have proposed using multispectral imagery as a vehicle for stationary target detection. For example, Barry et al. (1977) have used a recursive state space filtering technique with multispectral images to reduce background clutter, hence improving target detectability (Barry et al., 1977a & b). More recently, Margalit et al. (1984) developed a maximum likelihood (ML) approach to nonmoving resolved/partially resolved target extraction from correlated images. Specifically, they were able to detect known targets in clutter by performing an "optimum" weighted difference of locally demeaned[2], correlated multichannel subimages whose window dimensions are on the order of the target size (Margalit et al., 1984).

---

[1] The following references provide excellent reviews of current image processing trends and illustrate their utility for enhancing the inherent information content found in remotely sensed images such as those taken by LANDSAT and NIMBUS-7 satellites: Andrews and Hunt, 1972; Jerlov and Nielsen, 1974; Moik, 1978, 1979, and 1980; and Rosenfeld and Kak, 1982.

[2] In this report, demeaned refers to the removal of a local mean intensity from each pixel of an image.

This paper shows that the technique of Margalit et al. (1984) can be extended to the underresolved, weak target case by restructuring the basic problem development in terms of the inherent two-dimensional aspects found in most remotely sensed images. In particular, we wili present this restructured development and outline the research required to extend its application to an optimum processing approach for detecting stationary or slowly moving targets in clutter.

2. DUAL-CHANNEL TARGET DETECTION

A digital optical image is a two-dimensional array of numbers created by an optical sensor remotely sampling a continuous scene. The most common way of producing this type of data set is to optically image a scene through a lens system onto a photodetector array. The electrical signal generated by this detector array is then sent through an analog-to-digital converter, and the result is either image-processed immediately, or stored in a nonvolatile medium like magnetic tape for future analysis. The digital signal's most important property is that each generated element is always greater than, or equal to, zero. In this section, we will show how two specifically chosen digital images can be interacted to yield an optimum detection of an unknown signal, and we will discuss the necessary conditions to do so. For this development, we will assume the two images have dimensions equal to $(3N+1)\times(3N+1)$, with the unknown target potentially located within the center $(N+1)\times(N+1)$ portions of these arrays. As we will see later, our ML approach will reduce to working solely with $(N+1)\times(N+1)$ imagery, eliminating the need to waste a significant portion of any image array in future image statistics calculations.

Consider two image arrays $\underset{\sim}{f}$ and $\underset{\sim}{g}$ that contain two registered, correlated scenes, respectively. Assume that $\underset{\sim}{f}$ may or may not contain an additional intensity distribution $\underset{\sim}{s}$, where $\underset{\sim}{s}$ is not strong enough to alter $\underset{\sim}{f}$'s inherent statistics but is above any quantization or other system-level noise. Arrays $\underset{\sim}{f}$ and $\underset{\sim}{s}$ do not necessarily have the same dimensions. The intensity array $\underset{\sim}{s}$ represents the signal we wish to extract from the background clutter found in $\underset{\sim}{f}$. Physically, these images could be produced by either a multispectral scanning array sensor, a dual-channel staring mosaic array sensor, or a normal array sensor sampled at two different times. We begin our analysis by transforming each centered $(N+1)\times(N+1)$ subimage of $\underset{\sim}{f}$ and $\underset{\sim}{g}$ into their lexicographic form. Specifically, we write

$$\underset{\sim}{f} = \begin{pmatrix} f(N,N) \\ f(N,N+1) \\ \vdots \\ f(N+1,N) \\ \vdots \\ f(2N,2N) \end{pmatrix} \tag{1a}$$

$$\underset{\sim}{g} = \begin{pmatrix} g(N,N) \\ g(N,N+1) \\ \vdots \\ g(N+1,N) \\ \vdots \\ g(2N,2N) \end{pmatrix} \tag{1b}$$

Since we are dealing with target detection from multiple observations, these vectors can now be merged into multivariate form

$$\underset{\sim}{h} = \begin{matrix} \underset{\sim}{f} \\ \underset{\sim}{g} \end{matrix} \tag{2}$$

to facilitate further analysis.

ML signal processing is optimum when one is dealing with noise (i.e., background clutter), which is described by stationary, white Gaussian statistics. Unfortunately, most optical imagery is quasistationary, colored, and non-Gaussian. This situation can be remedied to a certain degree by subtracting a local neighborhood mean from each of the elements found in $\underset{\sim}{h}$ (Margalit et al., 1984; Hunt & Cannon, 1976). We shall discuss this point in more detail in the following section and ask the reader to assume for the present that one can construct a difference vector $(\underset{\sim}{h}-\underset{\sim}{h}')$ that has a multivariate normal probability density function with a zero mean and a covariance $\underset{\sim}{\underset{\sim}{R}}$. The covariance matrix $\underset{\sim}{\underset{\sim}{R}}$ is described by the relation

$$\underset{\sim}{\underset{\sim}{R}} = E[(\underset{\sim}{h}-\underset{\sim}{h}')(\underset{\sim}{h}-\underset{\sim}{h}')^T] \tag{3}$$

and is calculated using a $(N+1)\times(N+1)$ window. Specifically, the elements of $\underset{\sim}{\underset{\sim}{R}}$ would be calculated as follows: returning to the original two images, one would derive a local neighborhood mean for each pixel contained in $\underset{\sim}{f}$ and $\underset{\sim}{g}$ and form two new image arrays given by $(\underset{\sim}{f}-\underset{\sim}{f}')$ and $(\underset{\sim}{g}-\underset{\sim}{g}')$. Here, the primed letters indicate the estimated mean array for its associated image. Mathematically, they can be written as

$$\underset{\sim}{f}' = E[\underset{\sim}{f}]$$

and

$$\underset{\sim}{g}' = E[\underset{\sim}{g}]$$

for the two images $\underset{\sim}{f}$ and $\underset{\sim}{g}$, respectively. In the above two equations, E[...] denotes the expectation or expected value operator, which will not, in general, result in constant valued vectors. Given these two new images, one can then calculate the autocovariance matrices for $(\underset{\sim}{f}-\underset{\sim}{f}')$ and $(\underset{\sim}{g}-\underset{\sim}{g}')$, as well

as their covariance matrix for the center (N+1)×(N+1) portions of both arrays. Since these calculations involve summing products of pixel values over (N+1)×(N+1) windows, this explains our initial requirement of having overall image dimensions of (3N+1)×(3N+1). The first row of $\underset{\sim}{\underset{\sim}{R}}$ is equal to

$$R(0,k) = E[(f(N,N)-f'(N,N))\times(f(N,N+k)-f'(N,N+k))]$$

$$R(0,N+1+k) = E[(f(N,N)-f'(N,N))\times(f(N+1,N+k)-f'(N+1,N+k))]$$

$$R(0,2N+1+k) = E[(f(N,N)-f'(N,N))\times(f(N+2,N+k)-f'(N+2,N+k))]$$

etc.

$$R(0,(N-1)\times N+1+k) = E[(f(N,N)-f'(N,N))\times(f(2N,N+k)-f'(2N,N+k))]$$

for k between 0 and N. In these expressions, we have

$$E[(f(m,n)-f'(m,n))\times(f(k,l)-f'(k,l))] =$$

$$\sum_i \sum_j (f(m+i,n+j)-f'(m+i,n+j))\times(f(k+i,l+j)-f'(k+i,l+j)) \quad . \qquad (4)$$

The second row of $\underset{\sim}{\underset{\sim}{R}}$ is given by

$$R(1,k) = E[(f(N,N+1)-f'(N,N+1)\times(f(N,N+k)-f'(N,N+k))]$$

$$R(1,N+1+k) = E[(f(N,N+1)-f'(N,N+1))\times(f(N+1,N+k)-f'(N+1,N+k))]$$

$$R(1,2N+1+k) = E[(f(N,N+1)-f'(N,N+1))\times(f(N+2,N+k)-f'(N+2,N+k))]$$

etc.

$$R(1,(N-1)\times N+1+k) = E[(f(N,N+1)-f'(N,N+1))\times(f(2N,N+k)-f'(2N,N+k))]$$

for k between 0 and N. Here

$$E[(f(m,n)-f'(m,n))\times(g(k,l)-g'(k,l))] =$$

$$\sum_i \sum_j (f(m+i,n+j)-f'(m+i,n+j))\times(g(k+i,l+j)-g'(k+i,l+j)) \quad . \qquad (5)$$

This procedure continues until all the elements of the ($\underset{\sim}{f}$-$\underset{\sim}{f}$') portion of ($\underset{\sim}{h}$-$\underset{\sim}{h}$') have been used. This procedure continues until all the elements of the

($\underset{\sim}{g}$-$\underset{\sim}{g}'$) portion of ($\underset{\sim}{h}$-$\underset{\sim}{h}'$) have been used. One of the unexpected results Margalit et al. (1984) found from the subtraction of local neighborhood means from images was the transformation of the image vectors into white statistical processes (Margalit et al., 1984). That is, ($\underset{\sim}{f}$-$\underset{\sim}{f}'$) and ($\underset{\sim}{g}$-$\underset{\sim}{g}'$) have a Kronecker delta function autocovariance. This implies the covariance matrix reduces to a tridiagonal, symmetric matrix where the major diagonal terms are the scene variances and the minor diagonal terms are the aligned pixel covariances between the two scenes. If the scene variances are also slow-varying, this matrix further reduces to block Toeplitz matrix form. Let us now develop the maximum likelihood ratio for the target detection process.

Let H_0 represent the hypothesis that no signal $\underset{\sim}{s}'$ is present in ($\underset{\sim}{h}$-$\underset{\sim}{h}'$). The probability density function in this case is given by

$$P_0(\underset{\sim}{h}) = \frac{1}{(2\pi)^{2N+1}\det[\underset{\sim}{R}]} \exp\{-(\underset{\sim}{h}-\underset{\sim}{h}')^T \underset{\sim}{R}^{-1} (\underset{\sim}{h}-\underset{\sim}{h}')\} \tag{6}$$

where det[..] denotes the determinant of the enclosed matrix and $\underset{\sim}{R}^{-1}$ is the inverse of the covariance matrix R described above.

Let H_1 be the hypothesis that $\underset{\sim}{s}'$ is present in the vector (h-h'). Then the probability density function for this situation will be of the form

$$P_1(\underset{\sim}{h}) = \frac{1}{(2\pi)^{2N+1}\det[\underset{\sim}{R}]} \exp\{-(\underset{\sim}{h}-\underset{\sim}{h}'+\underset{\sim}{s}')^T \underset{\sim}{R}^{-1} (\underset{\sim}{h}-\underset{\sim}{h}'+\underset{\sim}{s}')\} \tag{7}$$

with $\underset{\sim}{s}'$ defined as

$$\underset{\sim}{s}' = \begin{pmatrix} s(N,N) \\ \vdots \\ s(2N,2N) \\ 0 \\ \vdots \\ 0 \end{pmatrix} .$$

Taking the ratio of these last two equations, we are able to formulate the best test for establishing the presence of the signal $\underset{\sim}{s}'$, given a fixed false alarm probability. This test is known as the likelihood ratio test and is given by

$$\Lambda = P_1(\underset{\sim}{h})/P_0(\underset{\sim}{h}) \begin{cases} > = K ; & \text{for } \underset{\sim}{s}' \text{ being present in } (\underset{\sim}{h}-\underset{\sim}{h}') \\ < \quad K ; & \text{for } \underset{\sim}{s}' \text{ being absent in } (\underset{\sim}{h}-\underset{\sim}{h}') \end{cases}$$

where K is a constant to be determined. Taking the logarithm of Λ, we obtain

$$-(\underset{\sim}{h}-\underset{\sim}{h}'+\underset{\sim}{s}')^T \underset{\approx}{R}^{-1} (\underset{\sim}{h}-\underset{\sim}{h}'+\underset{\sim}{s}') + (h-h')^T \underset{\approx}{R}^{-1} (\underset{\sim}{h}-\underset{\sim}{h}') \begin{matrix} < K'; \text{ signal absent} \\ \geq K'; \text{ signal present} \end{matrix} \qquad (8)$$

as our statistical test. For the remainder of this development, let us assume the covariance matrix R is of block Toeplitz form and the signal is totally confined to a single pixel. This can be done without loss of generality and will greatly simplify the discussion to come.

Under the above assumption of a slowly varying covariance matrix, we can easily show that the inverse covariance matrix R is given by

$$\underset{\approx}{R}^{-1} = \begin{pmatrix} \sigma'_f & 0 & \cdots & 0 & R'_{fg} & 0 & \cdots & 0 \\ 0 & \sigma'_f & \cdots & 0 & R'_{fg} & 0 & \cdots & 0 \\ \vdots & \vdots & & \vdots & \vdots & \vdots & & \vdots \\ R'_{fg} & 0 & \cdots & \sigma'_g & 0 & \cdots & 0 & R'_{fg} \\ 0 & R'_{fg} & \cdots & 0 & \sigma'_g & 0 & \cdots & 0 \\ \vdots & & & & & & & \vdots \\ 0 & \cdots & R'_{fg} & 0 & 0 & \cdots & 0 & \sigma'_g \end{pmatrix} \qquad (9)$$

where

$$\sigma_f' = \frac{1}{\sigma_f^2(1-\rho^2)} \tag{10}$$

$$\sigma_g' = \frac{1}{\sigma_g^2(1-\rho^2)}$$

$$R_{fg}' = \frac{-\rho}{\sigma_f\sigma_g(1-\rho^2)} \quad .$$

In these equations, σ_f^2 and σ_g^2 denote the scene variances of $(\underset{\sim}{f}-\underset{\sim}{f}')$ and $(\underset{\sim}{g}-\underset{\sim}{g}')$, respectively, and ρ the correlation between the two images. If the signal is located in pixel (M_0,N_0) where $N < M_0,N_0 < 2N$, the left hand side of equation 8 becomes

$$\frac{(\underset{\sim}{f}-\underset{\sim}{f}'+\underset{\sim}{s}')^2}{\sigma_f^2(1-\rho^2)} - \frac{2\rho(\underset{\sim}{f}-\underset{\sim}{f}'+\underset{\sim}{s}')(\underset{\sim}{g}-\underset{\sim}{g}')}{\sigma_f\sigma_g(1-\rho^2)} + \frac{(\underset{\sim}{g}-\underset{\sim}{g}')^2}{\sigma_g^2(1-\rho^2)} - \frac{(\underset{\sim}{f}-\underset{\sim}{f}')^2}{\sigma_f^2(1-\rho^2)}$$

$$+ \frac{2\rho(\underset{\sim}{f}-\underset{\sim}{f}')(\underset{\sim}{g}-\underset{\sim}{g}')}{\sigma_f\sigma_g(1-\rho^2)} - \frac{\rho^2(\underset{\sim}{g}-\underset{\sim}{g}')^2}{\sigma_g^2(1-\rho^2)}$$

$$= \frac{(\underset{\sim}{f}-\underset{\sim}{f}'+\underset{\sim}{s}')}{\sigma_f(1-\rho^2)} - \frac{2\rho(\underset{\sim}{f}-\underset{\sim}{f}'+\underset{\sim}{s}')(\underset{\sim}{g}-\underset{\sim}{g}')}{\sigma_f\sigma_g(1-\rho^2)} + \frac{\rho^2(\underset{\sim}{g}-\underset{\sim}{g}')^2}{\sigma_g^2(1-\rho^2)}$$

$$- \frac{(\underset{\sim}{f}-\underset{\sim}{f}')}{\sigma_f(1-\rho^2)} + \frac{2\rho(\underset{\sim}{f}-\underset{\sim}{f}')(\underset{\sim}{g}-\underset{\sim}{g}')}{\sigma_f\sigma_g(1-\rho^2)} - \frac{\rho^2(\underset{\sim}{g}-\underset{\sim}{g}')^2}{\sigma_g^2(1-\rho^2)} \tag{11}$$

$$= \frac{\left[(\underset{\sim}{f}-\underset{\sim}{f}'+\underset{\sim}{s}') - \frac{\rho\sigma_f}{\sigma_g}(\underset{\sim}{g}-\underset{\sim}{g}')\right]^2}{\sigma_f^2(1-\rho^2)} - \frac{\left[(\underset{\sim}{f}-\underset{\sim}{f}') - \frac{\rho\sigma_f}{\sigma_g}(\underset{\sim}{g}-\underset{\sim}{g}')\right]^2}{\sigma_f^2(1-\rho^2)} \begin{matrix} < k' \\ \geq k' \end{matrix} \tag{12}$$

which reduces to

$$\frac{\left[(\underset{\sim}{f}-\underset{\sim}{f}'+\underset{\sim}{s}') - \frac{\rho\sigma_f}{\sigma_g}(\underset{\sim}{g}-\underset{\sim}{g}')\right]^2}{\sigma_f^2(1-\rho^2)} = \frac{|\underset{\sim}{s}'|^2}{\sigma_f^2(1-\rho^2)} \qquad \begin{matrix} < k' + 1 \\ \geq k' + 1 \end{matrix} \qquad (13)$$

under optimum subtraction. From this last equation we see that the identification and localization of a target signature within any image is totally dependent on the effective signal-to-noise ratio of the target in the weighted-difference image channel This is the type of detection criterion one usually finds for ML signal detections. However, there is another aspect to this target detection scheme one needs to consider. Let us be more specific.

The numerator of the first term of equation 13 can be interpreted as the apparent contrast of the target in the $(\underset{\sim}{f}-\underset{\sim}{f}')$ channel using an estimated mean from the $(\underset{\sim}{g}-\underset{\sim}{g}')$ channel. The ratio of the individual scene variances is the required scene weighting for optimum image subtraction. The denominator is the reduced scene variance obtained from dual-channel weighted differencing. Clearly, this last factor is very low for highly correlated channels and results in a potentially large signal-to-clutter/noise ratio in this case. However, it may not increase target detectability. The reason is an aspect of local neighborhood demeaning, which was not addressed by Margalit et al. (1984) and must hold if low false-alarm rates are desired. Specifically, the local neighborhood mean estimate must be chosen to minimize the difference between itself and the pixel it is demeaning, while minimally affecting the target signature. In other words, the second-order moments of $(\underset{\sim}{f}-\underset{\sim}{f}')$ and $(\underset{\sim}{g}-\underset{\sim}{g}')$ must be minimized, in addition to their third-order moments, if one expects to optimally differentiate weak signals from residual clutter in the dual-channel weighted-difference channel.

3. KEY MAXIMUM LIKELIHOOD PROCESSING ASSUMPTIONS

In the previous section, we found that a ML target detection technique was applicable to dual-channel imagery if certain fundamental noise characteristics were present. Specifically, we require the locally demeaned background clutter to be

a. Stationary

b. White

c. Gaussian distributed

d. Very close to zero variance.

These conditions are essential to successful implementation of the ML method for underresolved, weak target localization in remotely sensed data. Ancillary to these points is the assumption that the multispectral images involved in the processing are registered perfectly. In this section, we shall discuss these points in more detail, focusing on how they pertain to real imagery.

From Helstrom (1968), we know that ML detection of known signals in clutter is an optimum process when the noise involved is stationary and white Gaussian. In addition, the previous mathematical development illustrates that it is highly desirable for the two locally demeaned images to have as small a standard deviation as possible to reduce potential false alarms. In contrast, raw optical imagery rarely has these properties and must be modified if one wishes to apply the ML approach to target detection. Hunt and Cannon (1976) suggested that an image can be transformed into the desired statistical state by the appropriate demeaning process. They showed for one particular image that a neighborhood average estimate of a local pixel mean could be subtracted

from each individual pixel to yield a nearly Gaussian probability density function for the resultant scene. However, the exact pixel weighting criteria for optimum mean estimations was not discussed; therefore, only a pixel blurring estimation was obtained.

Margalit et al. (1984) used an equal-weight neighborhood average and varied array size, i.e., 3 by 3, 5 by 5, 7 by 7, etc., to yield the most Gaussian fit. The criterion used was minimization of the absolute value of the third-order moment of the demeaned image. No specific numbers for this moment were cited in the reference, but a number of statistical tests were used to establish normality. Their conclusion from this point of analysis was the equal-weight neighborhood average estimation yielded nearly, but not totally, Gaussian distributions. In fact, the authors suggested that the resulting intensity histograms were more closely fit by the weighted sum of Gaussian and uniform distributions. Let us see what type of third-moment minimization occurs when an equal-weight neighborhood average mean estimation is applied to some typical infrared imagery.

Figure 1[3] shows an infrared image of downtown San Jose and its associated intensity histogram. These data were obtained with a DAEDALUS thermatic mapper housed in a National Aeronautics and Space Administration U-2 aircraft by using eight-bit quantization. The pixel footprint size is of the order of 30 by 30 meters. Table 1 gives the first four moments, the skewness, and the kurtosis of the scene's intensity statistics, as well as the center 11 by 11 portion of the autocovariance matrix for the 482- by 482-pixel image. In this

---

[3] Because of the large number of figures and tables in this report relative to the amount of text, these illustrations are placed at the end of the report beginning on page 15.

table, each element of the autocovariance matrix has been multiplied by 100. The histogram plot and table 1 show that the scene statistics are non-Gaussian. The intensity statistics are skewed and possess a large, negative third-order moment.

Figures 2 through 7 depict the resulting scenes and associated intensity histograms for locally demeaned versions of figure 1 using window sizes of 3 by 3, 5 by 5, 7 by 7, 9 by 9, 11 by 11, and 13 by 13, respectively. Tables 2 through 7 summarize the key image statistics of these figures. Comparisons of the figures and tables show that equal-weight mean estimation produces imagery that is smaller in scene variance and nearly white Gaussian. That is, each of the demeaned images have first-order moments close to zero, reduced variance, delta-function like autocovariances, and intensity distributions that appear symmetrical in shape. These properties degrade with increasing window size. The degradation is a consequence of the larger window sizes performing a poor quality, low-pass filtering estimate of the local mean. They are actually estimating a more global-like image mean. In any event, the third-order moment never really approaches a value close to zero for any of these windows, as required for a Gaussian probability density function. Based on the Margalit et al. (1984) criteria: the 3- by 3-averaging window would be selected as the optimum processing window. This can be seen by comparing the third-order moments found in tables 2 through 7 and by observing that the absolute value of -23.68 in table 2 is smallest. However, this is still a large value and suggests that the 3 by 3 window does not yield as good a Gaussian PDF as one would like for optimum ML processing.

Figure 8 is a DAEDALUS image of Los Gatos and its surrounding mountain area. Its intensity frequency distribution is clearly more non-Gaussian than the San Jose scene. Table 8 depicts the key image statistics for the image

and the center 11 by 11 portion of its autocovariance matrix. Figures 9 through 11 and the associated intensity histograms are the resulting images generated by equal-weight mean estimation subtraction using 3- by 3-, 5- by 5-, and 7- by 7-processing windows, respectively. Tables 9 through 11 summarize the key image statistics of these figures, respectively. As before, the resulting images appear to possess nearly Gaussian intensity distributions, which degrade with increasing window size. However, the second- and third-order moments are now both nonzero positive in all cases. (Recall for the San Jose image that the third-order moment was nonzero negative for the five processing windows used). Hence, the application of ML target detection to the optimum demeaned Los Gatos image (again created by a 3- by 3-processing window) will suffer from the same nonoptimum conditions we found for the San Jose scene.

Another key assumption in the previous ML development is the requirement that two registered images be available for processing. Optical sensor systems are not able to stare at a point perfectly, but have long- and short-term drifts, as well as a jitter, affecting the scene positioning from one instant to another. The impact of any misregistration between the two images is presently not known.

4. TOPICS FOR FURTHER INVESTIGATION

Besides the points discussed in the previous section, two additional areas remain to be investigated to clearly establish the optimum application of ML detection to optical imagery. One is to determine the best low-pass filter for local neighborhood mean estimation; the other is the effect of scene misregistration on ML image processing. For the former, we propose

using least mean-square estimation to determine the best convolutional filter for approximating the local mean about any one pixel. This will be done theoretically, assuming typical image autocovariance functions, and experimentally with real visible and infrared data. Comparisons between the two approaches will be made. To assess the impact of scene misregistration on ML image processing, we propose a theoretical investigation of this effect using known image autocovariance functions and various means of image sampling. Computer simulations will be used to verify results.

In addition to these areas, we suggest that the technique described in section 2 be extended to more than two spectral channels to determine if any additional improvement can be gained and, if so, under what conditions. Example images from the LANDSAT and DAEDALUS can be used to verify these projections

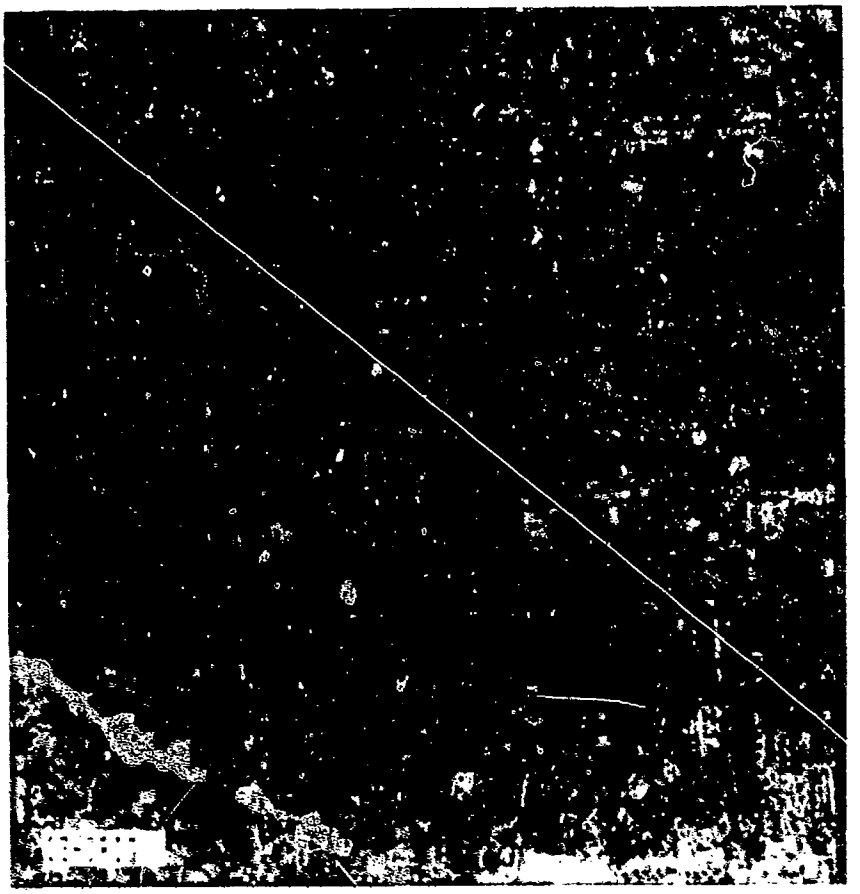

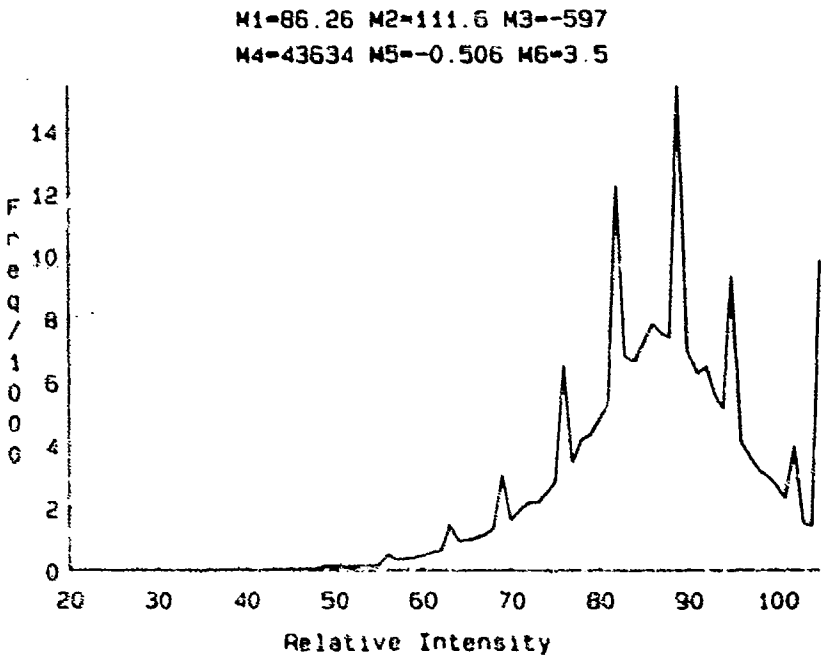

Figure 1. Original image of downtown San Jose and associated intensity histogram

Table 1. Key statistical parameters for the original image of downtown San Jose.

First-order moment (mean) = 86.2607

Second-order moment (variance) = 111.5682

Third-order moment = -597.0149

Fourth-order moment = 43634.3333

Skewness = -0.5066

Kurtosis = 3.5054

26	27	29	31	35	37	33	31	29	28	26
26	28	30	32	36	38	35	32	30	29	27
27	30	32	35	41	45	40	35	32	30	28
29	32	34	39	46	52	46	39	35	32	29
29	33	36	41	53	67	55	42	36	33	29
34	38	43	50	73	100	73	50	43	38	33
30	33	37	42	55	67	53	41	36	32	29
30	33	35	39	46	55	46	39	34	31	28
29	31	33	36	40	45	41	35	32	30	27
28	30	31	33	35	39	36	32	30	28	26
27	29	30	32	34	37	35	31	29	27	26

Center 11×11 Autocovariance matrix (×100)

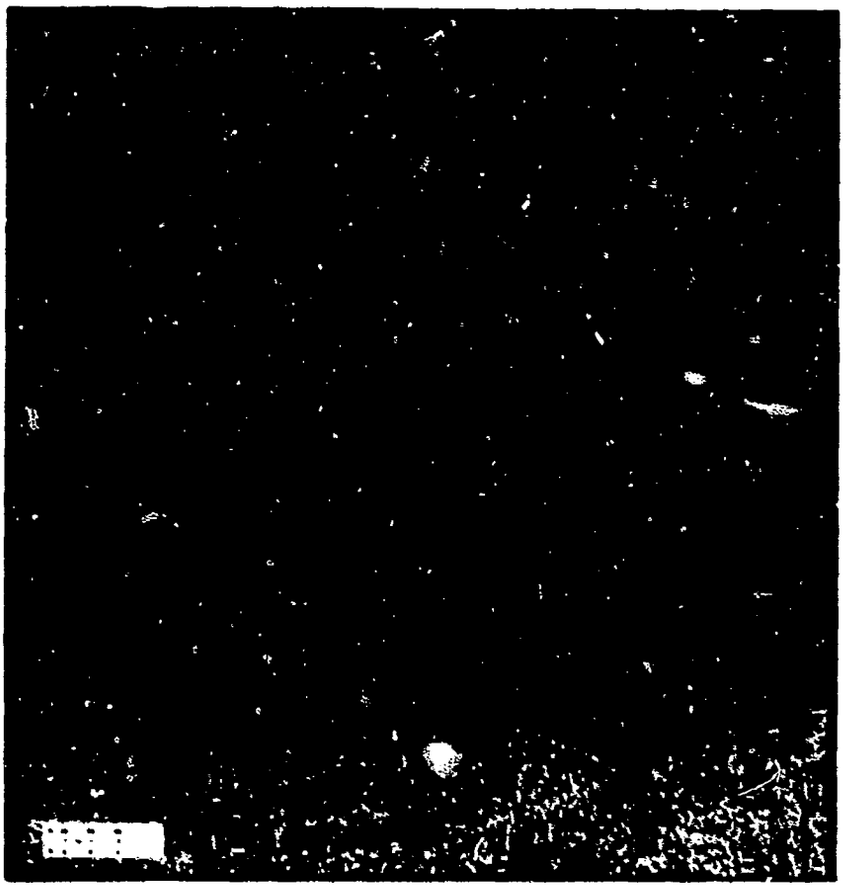

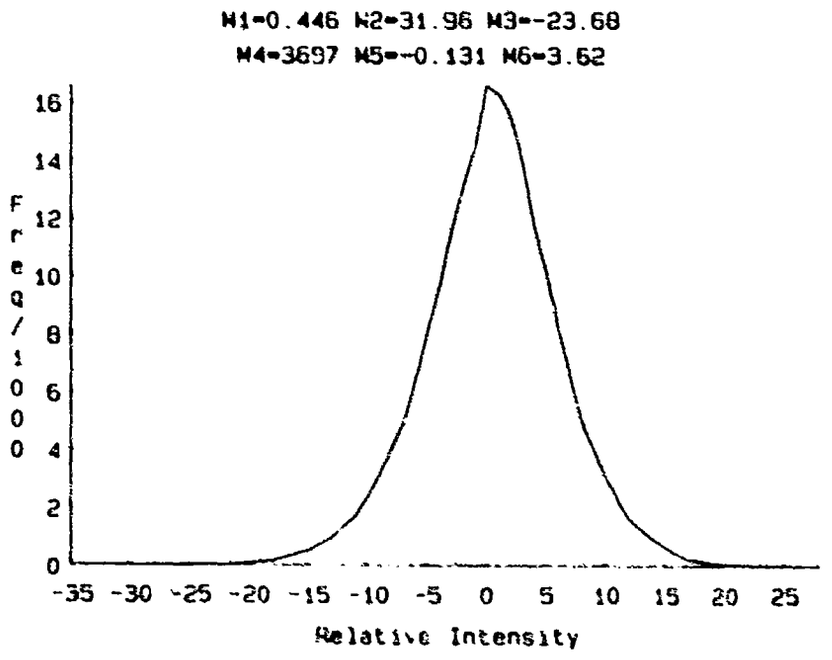

Figure 2 The 3 by 3 demeaned image of downtown San Jose and associated intensity histogram.

Table 2. Key statistical parameters for the 3- by 3-demeaned image of downtown San Jose.

First-order moment (mean) = 0.4461

Second-order moment (variance) = 31.9559

Third-order moment = -23.6814

Fourth-order moment = 3697.4117

Skewness = -0.1310

Kurtosis = 3.6207

2	1	2	2	5	9	2	3	2	2	1
0	0	-1	-4	-5	0	-6	-2	-1	0	-1
-1	1	0	-1	0	8	-2	-1	-1	1	0
2	3	3	3	0	11	-2	2	4	4	1
-7	-7	-8	-19	-36	-8	-30	-19	-9	-7	-7
8	13	16	9	29	100	29	9	16	13	9
-7	-7	-9	-19	-30	-8	-36	-19	-8	-7	-7
1	4	4	2	-2	11	0	3	3	3	2
0	1	-1	-1	-2	8	0	-1	0	1	-1
-1	0	-1	-2	-6	0	-5	-4	-1	-1	-1
1	2	2	3	2	9	5	2	2	2	2

Center 11×11 Autocovariance matrix (×100)

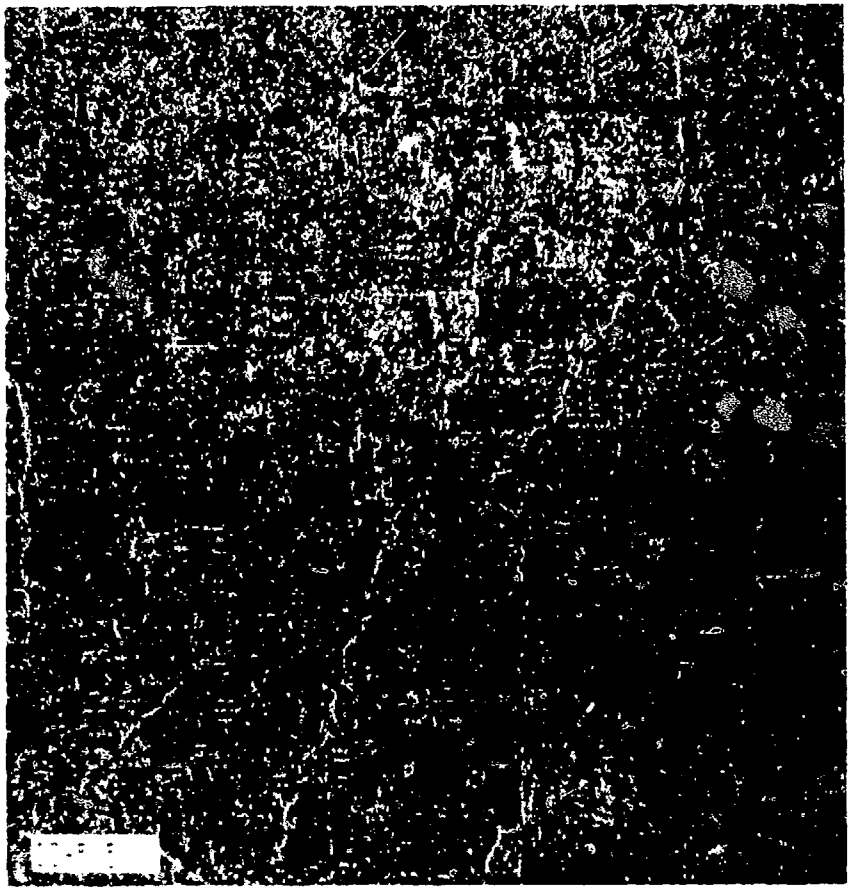

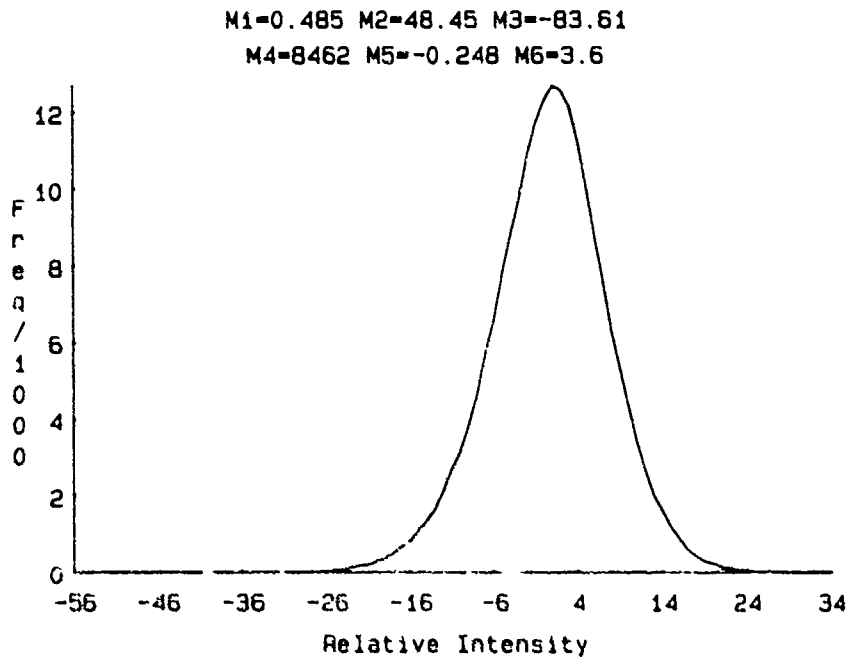

Figure 3. The 5- by 5-demeaned image of downtown San Jose and associated intensity histogram.

Table 3. Key statistical parameters for the 5- by 5-demeaned image of downtown San Jose.

First-order moment (mean) = 0.4849

Second-order moment (variance) = 48.4504

Third-order moment = -83.6112

Fourth-order moment = 8462.3295

Skewness = -0.2479

Kurtosis = 3.6049

2	2	0	-1	4	8	1	-1	1	2	1
1	1	-1	-4	0	5	-2	-4	0	1	0
0	2	-1	-6	1	8	-2	-7	-1	2	1
-2	-1	-7	-18	-11	1	-13	-18	-6	0	-2
-2	0	-7	-21	-6	25	-1	-19	-7	0	-2
7	12	7	-2	39	100	39	-2	8	12	7
-2	0	-7	-19	-1	25	-6	-21	-7	0	-2
-2	0	-6	-19	-13	1	-11	-18	-7	-1	-2
1	2	-1	-7	-2	8	1	-6	-1	2	0
0	1	0	-4	-2	5	0	-5	-1	1	0
1	2	1	-1	1	8	5	-1	0	2	2

Center 11×11 Autocovariance matrix (×100)

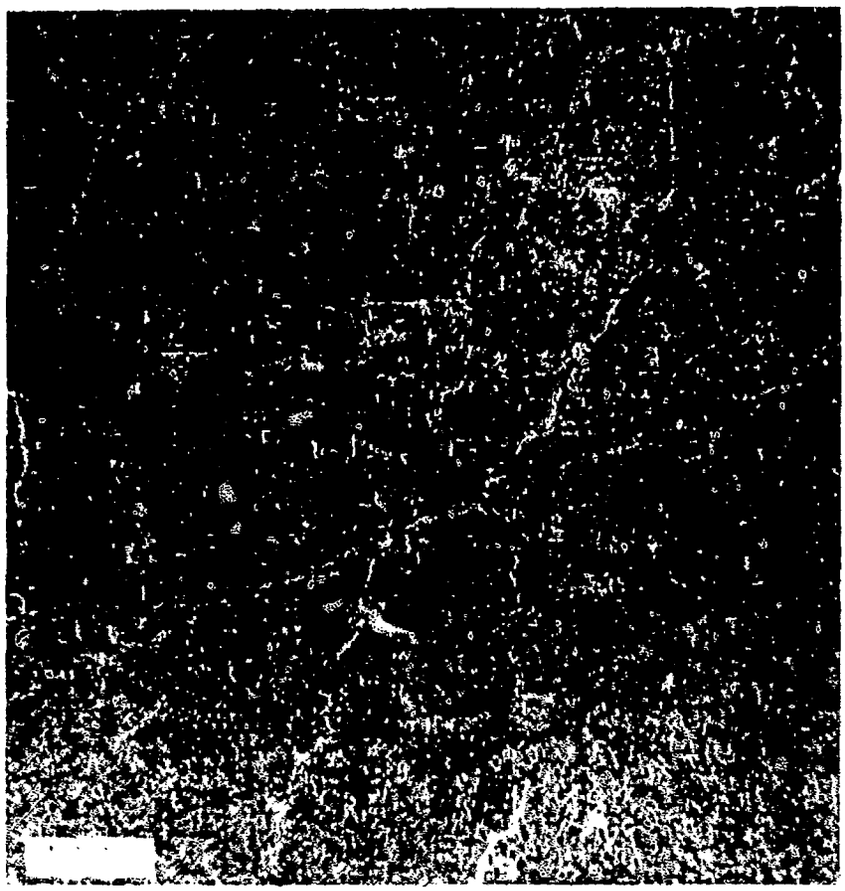

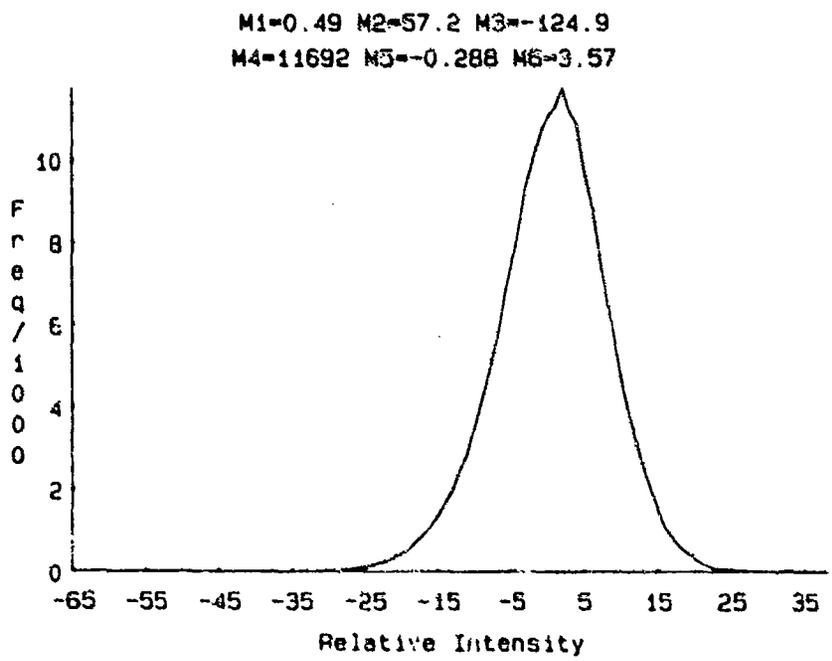

Figure 4. The 7- by 7-demeaned image of downtown San Jose and associated intensity histogram.

Table 4. Key statistical parameters for the 7- by 7-demeaned image of downtown San Jose.

First-order moment (mean) = 0.4958

Second-order moment (variance) = 57.2018

Third-order moment = -124.9375

Fourth-order moment = 11692.8372

Skewness = -0.2887

Kurtosis = 3.5735

2	0	-2	0	5	9	2	-1	-1	2	2
1	-1	-5	-5	0	5	-2	-6	-5	0	1
-2	-5	-12	-13	-5	2	-7	-14	-12	-4	-1
-1	-4	-13	-12	-1	11	-2	-13	-12	-3	-1
-1	-4	-12	-11	9	36	13	-10	-11	-3	-1
7	7	1	5	48	100	48	5	1	7	7
0	-3	-11	-10	13	36	9	-11	-12	-3	-1
-1	-3	-12	-13	-2	11	-1	-12	-13	-4	-1
-1	-4	-13	-14	-7	2	-5	-13	-12	-5	-2
1	-1	-5	-6	-2	5	0	-5	-5	-1	1
2	2	-1	-1	2	9	5	0	-2	1	2

Center 11×11 Autocovariance matrix (×100)

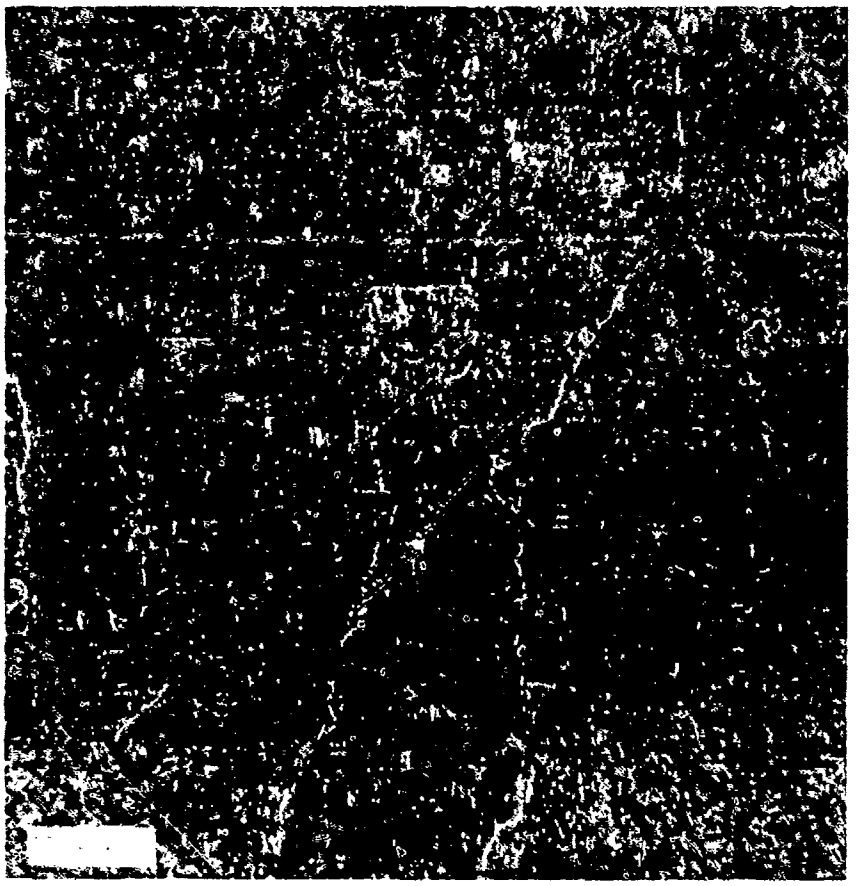

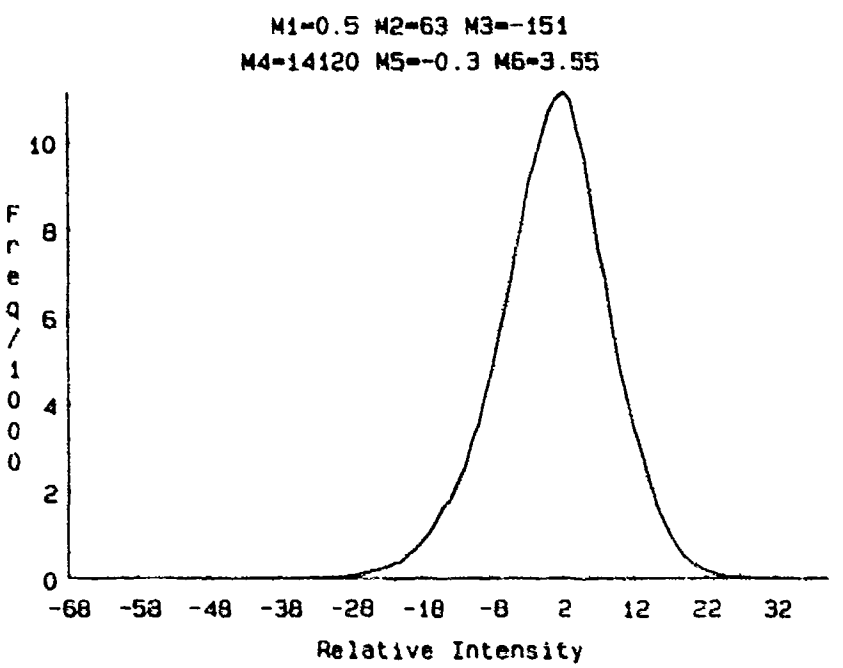

Figure 5. The 9- by 9-demeaned image of downtown San Jose and associated intensity histogram.

Table 5. Key statistical parameters for the 9- by 9-demeaned image of downtown San Jose.

First-order moment (mean) = 0.5004

Second-order moment (variance) = 63.0182

Third-order moment = -151.0908

Fourth-order moment = 14120.6381

Skewness = -0.3020

Kurtosis = 3.5556

-1	-3	-3	-1	4	7	1	-2	-3	-2	0
-4	-9	-10	-9	-3	0	-6	-9	-10	-8	-4
-6	-10	-11	-8	0	7	-2	-9	-11	-9	-4
-4	-9	-10	-4	7	17	6	-5	-9	-8	-4
-4	-8	-8	-2	16	41	20	-2	-8	-7	-3
3	2	4	13	53	100	53	13	4	2	4
-3	-8	-8	-2	20	41	16	-2	-8	-8	-4
-4	-8	-9	-5	6	17	7	-4	-10	-9	-4
-4	-9	-11	-9	-2	7	0	-8	-11	-10	-5
-4	-8	-11	-9	-6	0	-4	-9	-10	-9	-5
0	-2	-4	-2	1	7	4	-1	3	-3	0

Center 11×11 Autocovariance matrix (×100)

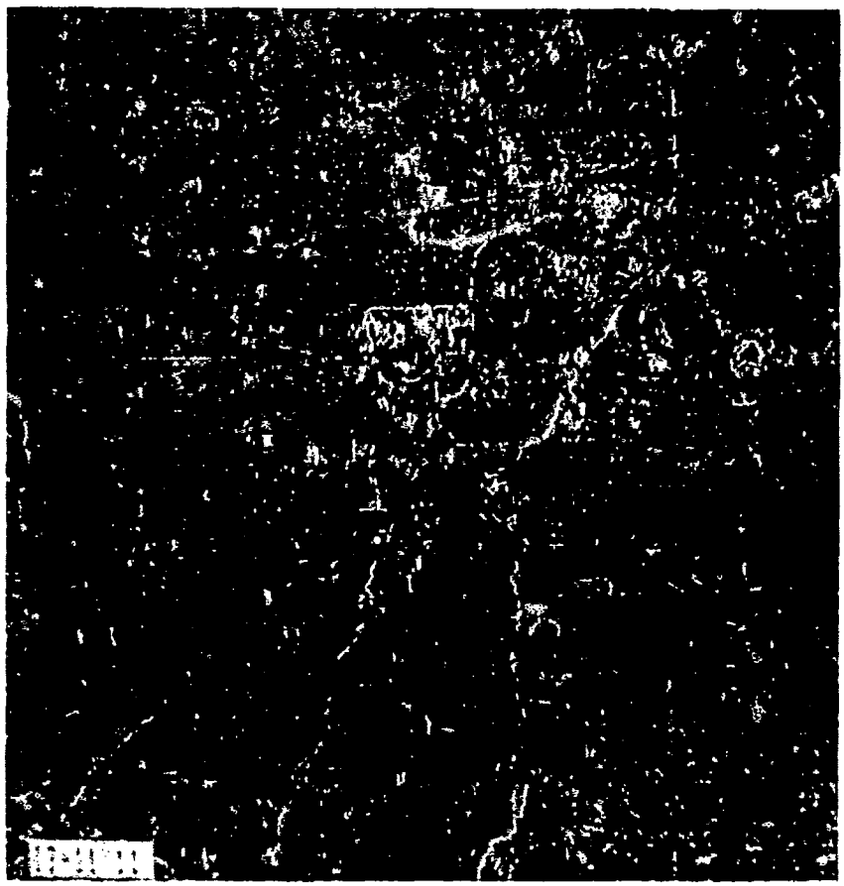

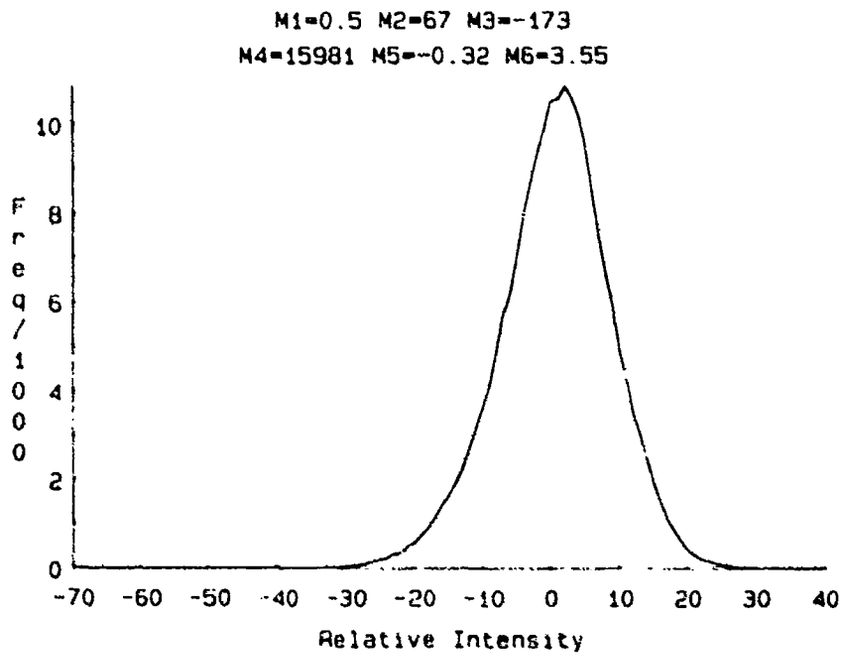

Figure 6. The 11-by 11-demeaned image of downtown San Jose and associated intensity histogram.

Table 6. Key statistical parameters for the 11- by 11-demeaned image of downtown San Jose.

First-order moment (mean) = 0.5023

Second-order moment (variance) = 67.0573

Third-order moment = -173.0976

Fourth-order moment = 15981.7429

Skewness = -0.3152

Kurtosis = 3.5541

-7	-8	-7	-4	1	4	-2	-5	-7	-7	-6
-9	-10	-9	-6	-1	3	-3	-7	-8	-9	-8
-9	-9	-8	-4	5	11	3	-4	-8	-8	-7
-8	-8	-5	1	12	22	11	1	-4	-6	-7
-7	-6	-3	4	22	45	25	4	-3	-6	-7
-1	2	7	17	55	100	55	17	8	3	0
-7	-6	-3	4	25	45	22	4	-3	-6	-7
-7	-7	-5	0	11	22	12	1	-5	-8	-8
-7	-8	-8	-4	3	11	5	-4	-8	-9	-9
-8	-9	-9	-7	-3	3	-1	-6	-9	-10	-9
-6	-7	-7	-5	-2	4	1	-4	-7	-8	-6

Center 11×11 Autocovariance matrix (×100)

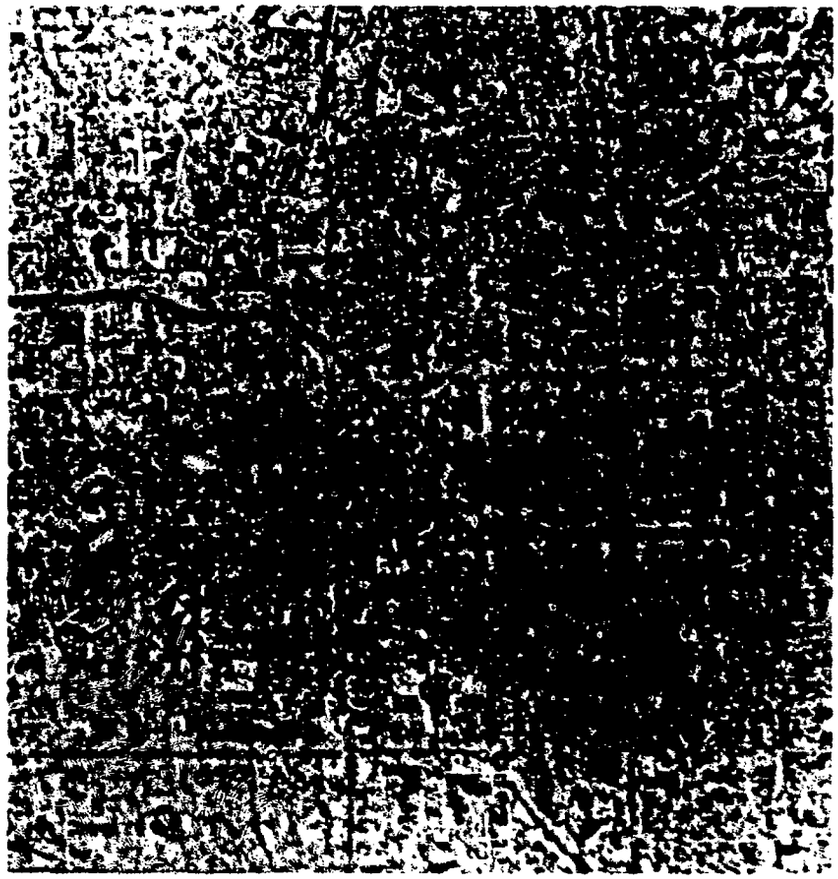

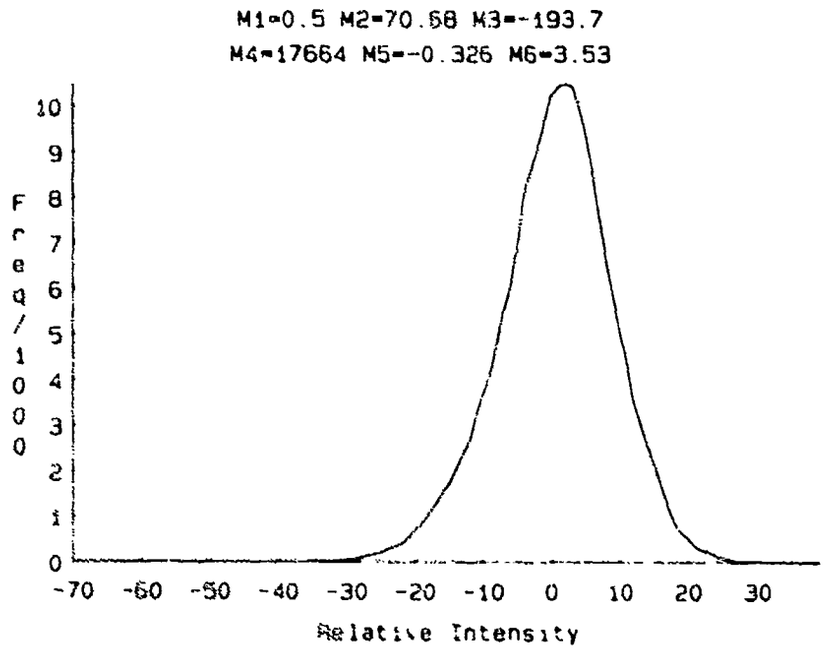

Figure 7. The 13- by 13-demeaned image of downtown San Jose and associated intensity histogram.

Table 7. Key statistical parameters for the 13- by 13-demeaned image of downtown San Jose.

First-order moment (mean) = 0.5023

Second-order moment (variance) = 70.6836

Third-order moment = -193.7154

Fourth-order moment = 17664.4662

Skewness = -0.3259

Kurtosis = 3.5355

-8	-7	-6	-3	2	5	0	-4	-6	-6	-7
-9	-8	-6	-4	2	6	0	-4	-6	-7	-8
-9	-7	-4	0	8	14	7	-1	-4	-6	-7
-7	-5	-2	5	16	26	15	5	0	-3	-7
-7	-4	0	7	25	47	28	8	1	-3	-6
0	5	11	21	57	100	57	21	11	5	0
-6	-3	1	8	25	47	25	7	0	-4	-7
-7	-4	-1	5	15	26	16	5	-1	-5	-7
-7	-6	-4	-1	7	15	8	0	-4	-7	-9
-8	-7	-6	-4	0	6	2	-4	-6	-8	-9
-7	-6	-6	-4	0	5	2	-3	-6	-7	-7

Center 11×11 Autocovariance matrix (×100)

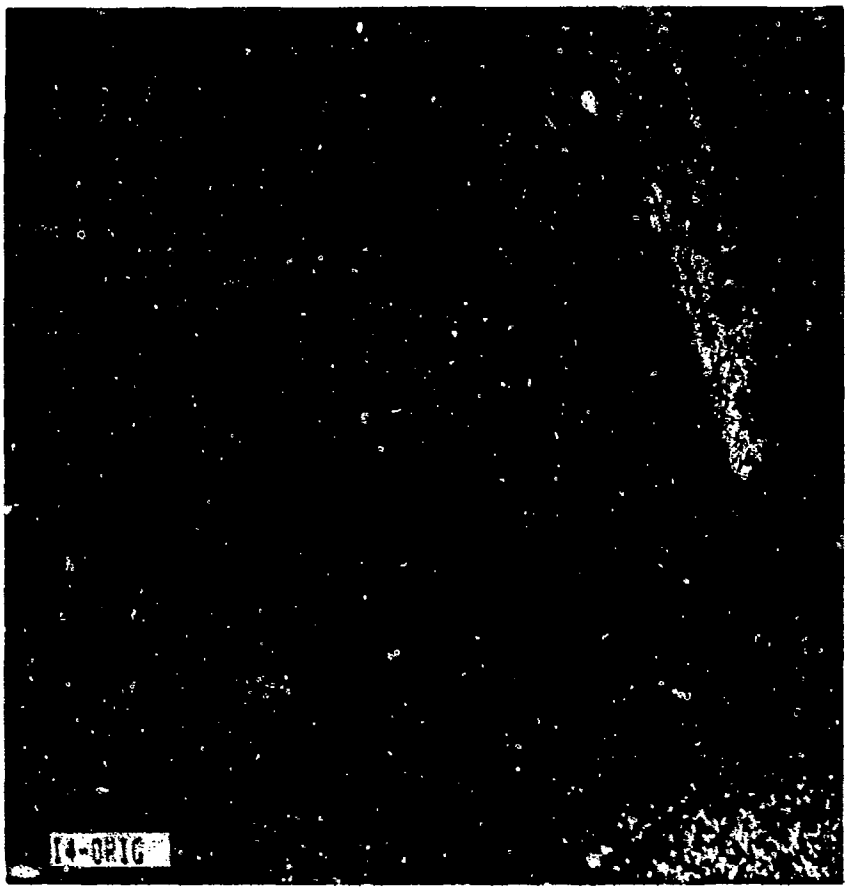

Figure 8. Original image of the Los Gatos area and associated intensity histogram.

Table 8. Key statistical parameters for the original image of Los Gatos/mountains.

First-order moment (mean) = 78.9999

Second-order moment (variance) = 749.8423

Third-order moment = 391.2464

Fourth-order moment = 1049415.4249

Skewness = 1.905E-02

Kurtosis = 1.8664

65	66	67	68	69	70	70	69	68	67	66
66	67	68	69	71	72	72	71	69	68	66
66	68	69	71	74	75	75	73	71	69	67
67	68	71	73	77	80	79	75	72	69	67
67	69	72	75	82	89	84	76	72	69	67
68	70	73	77	89	100	89	77	73	70	68
68	70	72	76	84	89	82	75	72	69	67
67	69	72	75	79	80	77	73	70	68	66
67	69	71	73	75	75	74	71	69	68	66
67	68	70	71	72	72	71	69	68	67	66
66	67	69	69	70	70	69	68	67	66	65

Center 11×11 Autocovariance matrix (×100)

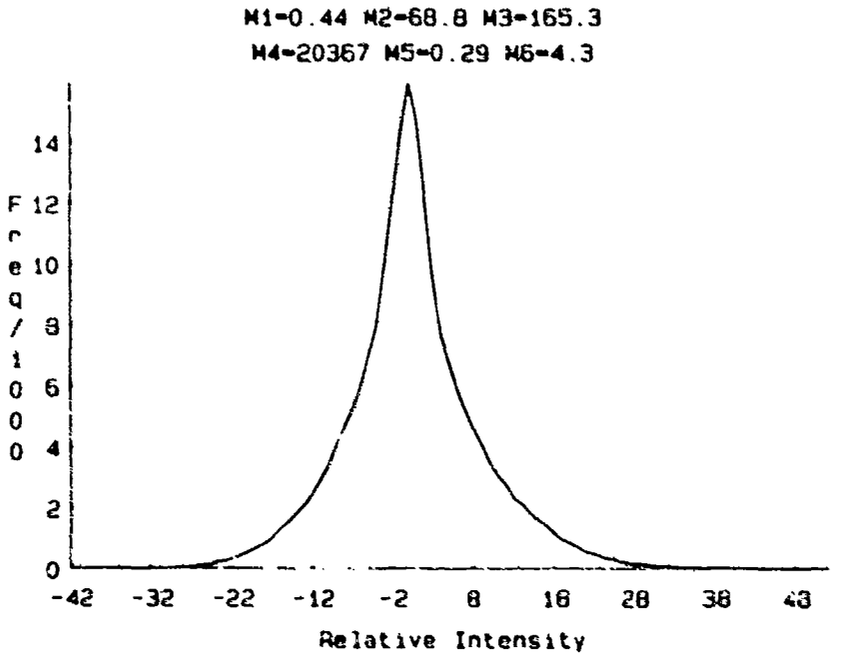

Figure 9. The 3 by 3 demeaned image of the Los Gatos area and associated histogram.

Table 9. Key statistical parameters for the 3- by 3-demeaned image of Los Gatos area.

First-order moment (mean) = 0.4445

Second-order moment (variance) = 68.8058

Third-order moment = 165.3608

Fourth-order moment = 20367.5595

Skewness = 0.2897

Kurtosis = 4.3021

1	2	1	1	1	2	1	1	1	1	0
-1	-1	-1	-3	-3	-1	-3	-3	-1	-1	-2
1	1	1	1	1	6	3	2	1	1	1
1	0	2	-1	-9	-2	-5	-2	1	0	0
-2	-3	-1	-14	-24	8	-15	-15	-2	-2	-2
3	4	7	-9	21	100	21	-9	7	4	3
-2	-2	-2	-15	-15	8	-24	-14	-1	-3	-2
0	0	1	-2	-5	-2	-9	-1	2	0	1
1	1	1	2	3	6	1	1	1	1	0
-2	-1	-1	-3	-3	-1	-3	-3	-1	-1	-1
0	1	1	1	1	2	1	1	1	2	1

Center 11×11 Autocovariance matrix (×100)

Figure 10. The 5- by 5-demeaned image of the Los Gatos area and associated histogram.

Table 10. Key statistical parameters for the 5- by 5-demeaned image of Los Gatos area.

First-order moment (mean) = 0.4803

Second-order moment (variance) = 125.1046

Third-order moment = 354.4667

Fourth-order moment = 64869.2644

Skewness = 0.2533

Kurtosis = 4.1446

1	1	0	-1	0	1	1	0	0	1	0
0	0	-1	-3	-2	2	0	-2	-1	0	-1
0	1	-1	-6	-4	2	0	-4	-2	0	0
-1	0	-6	-17	-14	-1	-7	-14	-7	-1	-1
-1	0	-7	-19	2	37	11	-16	-8	0	0
2	3	-3	-12	38	100	38	-12	-3	3	2
0	0	-8	-16	11	37	2	-19	-7	0	-1
0	-1	-7	-14	-7	-1	-14	-17	-6	0	-1
1	0	-2	-4	0	2	-4	-6	-1	1	0
-1	-1	-1	-2	0	2	-2	-3	-1	0	0
0	1	0	0	1	1	0	-1	0	1	1

Center 11×11 Autocovariance matrix (×100)

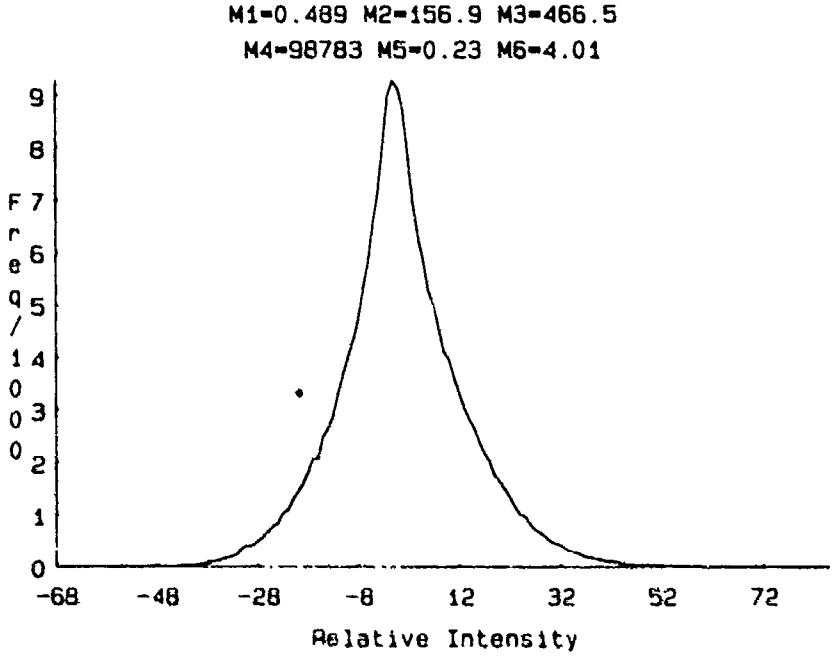

Figure 11. The 7- by 7-demeaned image of the Los Gatos area and associated histogram.

Table 11. Key statistical parameters for the 7- by 7-demeaned image of Los Gatos area.

First-order moment (mean) = 0.4892

Second-order moment (variance) = 156.9263

Third-order moment = 466.5482

Fourth-order moment = 98783.6512

Skewness = 0.2373

Kurtosis = 4.0113

1	0	-2	-3	-1	1	1	0	-1	0	0
0	-2	-6	-7	-5	0	-1	-4	-5	-3	-1
-1	-5	-11	-13	-7	0	-2	-8	-10	-5	-1
-1	-6	-13	-12	-2	10	5	-8	-12	-6	-1
-1	-6	-13	-8	19	49	27	-5	-12	-6	-1
1	-3	-9	-2	49	100	49	-2	-9	-3	1
-1	-6	-12	-5	27	49	19	-8	-12	-6	-1
-1	-6	-12	-8	5	10	-2	-12	-13	-6	-1
-1	-5	-10	-8	-2	0	-7	-13	-11	-5	-1
-1	-3	-5	-4	-1	0	-4	-7	-6	-2	0
0	0	-1	0	1	1	-1	-3	-2	0	1

Center 11×11 Autocovariance matrix (×100)

5. REFERENCES

Andrews, H.C. and Hunt, B.R. (1977). Digital Image Restoration. New York: Prentice-Hall.

Barry, P.E., Gran, R., and Waters, C.R. (1977a). State Variable Techniques in Optimal Image Processing. Conference on Image Science Mathematics, Naval Postgraduate School, Monterey, CA.

Barry, P.E., Gran, R., and Waters, C.R. (1977b). Optimal Recursive Filtering of Two Dimensional Processes. Asilomar Conference on Circuits and Systems: Asilomar, CA.

Helstrom, C.W. (1968). Statistical Theory of Signal Detection. (2d Ed.) New York: Pergamon Press.

Hunt, B.R. and Cannon, T.M. (1976). Nonstationary Assumptions for Gaussian Models of Images, 876-882. IEEE Trans. on Systems, Man. and Cybernetics.

Jerlov, N.G. and Nielsen, E.S. (1974). Optical Aspects of Oceanography. New York: Academic Press.

Margalit, A., Reed, I.S., and Gagliardi, R.M. (1984). Adaptive Detection of Stationary Optical and Infrared Targets using Correlated Scenes. (Tech. Rep. CSI-84-12-04) Communication Sciences Institute, University of Southern California.

Moik, J.G. (1978). Applications of Digital Signal Processing (Chap. 4). Oppenheim, A.V., Ed. New York: Prentice-Hall.

_____. (1979). Picture Processing and Digital Filtering, Huang, T.S., Ed., Topics in Applied Physics Series, (Vol. 6). New York: Springer-Verlag.

_____. (1980). Digital Processing of Remotely Sensed Images. (NASA SP-431). Washington, D.C.: National Aeronautics and Space Administration.

Rosenfeld, A. and Kak, A.C. (1982). Digital Picture Processing. (Vols. 1-2, 2d Ed.) New York: Academic Press.